Cyclonic eddies and upper thermocline fine-scale structures in the Antarctic Circumpolar Current

Harry Leach & Volker Strass

Ocean Dynamics
Theoretical, Computational and Observational Oceanography

ISSN 1616-7341

Ocean Dynamics
DOI 10.1007/s10236-018-1241-x

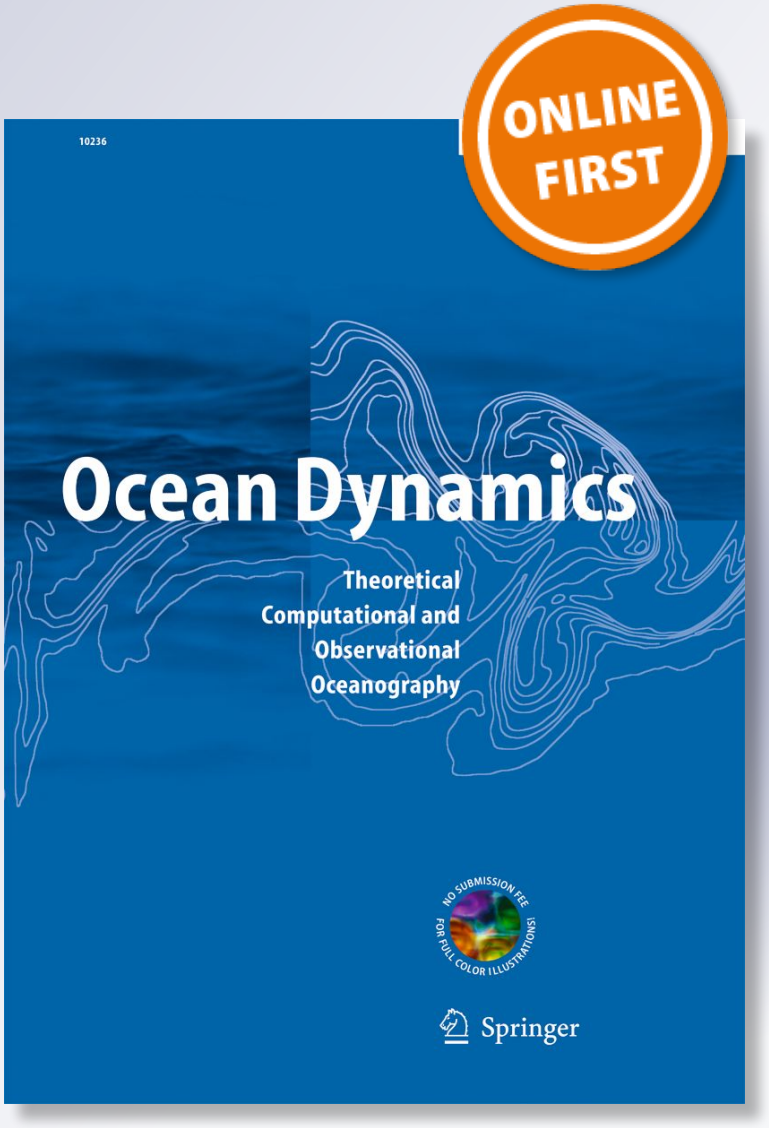

Springer

Ocean Dynamics
https://doi.org/10.1007/s10236-018-1241-x

Cyclonic eddies and upper thermocline fine-scale structures in the Antarctic Circumpolar Current

Harry Leach[1] · **Volker Strass**[2]

Received: 13 March 2018 / Accepted: 4 December 2018

Abstract

Mesoscale eddies in the open ocean are mostly formed by baroclinic instability, in which the available potential energy from the large-scale slope of the isopycnals is converted into the kinetic energy of the flow around the eddy. As a permissible form of motion within a rapidly rotating and stratified fluid eddies driven by baroclinic instability are important for the poleward and vertical transport, not only of physical properties, but also biogeochemical ones. In this paper, we present observations from four cyclonic eddies in the Antarctic Circumpolar Current. We have sorted them by apparent age, based on altimeter data and consideration of the degree of homogenisation of the potential temperature-salinity(θS) relationship, and then looked at the spatial distribution of measures of fine-scale variability in the upper thermocline. The youngest eddy shows isopycnals which are domed upwards and it contains a variety of waters with differing temperature-salinity characteristics. The fine-scale variability is higher in the core of the eddy. The older eddies show a core which is more homogeneous in potential temperature and salinity. The isopycnals are flatter in the centre of the eddy, and in cross-section, they can be M-shaped, so that the steepest gradients are concentrated around the edge. The fine-scale variability is more concentrated around the edges where the density gradients are stronger. We hypothesise that lateral stirring and mixing processes within the eddy homogenise the water so that the temperature-salinity relationship becomes tighter. When the eddy eventually collapses, this modified water can be released back into the flow. Thus, we see how the interplay of mesoscale and small-scale processes are modifying water mass properties and, potentially, regulate biogeochemical processes.

Keywords Mesoscale eddies · Fine-scale structures · Antarctic Circumpolar Current

1 Introduction

Mesoscale eddies in the open ocean are generally formed by baroclinic instability, in which the available potential energy from the large-scale slope of the isopycnals is converted into the kinetic energy of the flow around the eddy. Work on eddies began in the atmosphere with theories of baroclinic instability being evolved in the 1940s (Charney 1947; Eady 1949) to explain synoptic scale weather systems. At this time, oceanographers were more concerned with understanding the basin-scale wind-driven gyres (Sverdrup 1947; Stommel 1948; Munk 1950). When, however, oceanographers tried to observe this slow, steady, large basin-scale flow ($\sim$cm s^{-1}) they found that it was masked by much stronger variable flow ($\sim$10 s cm s^{-1}) on smaller scales, 10 s to 100 s km. This led to the Mid-Ocean Dynamics Experiment 1973 (MODE-Group 1978) and the realisation that baroclinic instability was also important in the ocean (Gill et al. 1974).

The initial instability theories were only concerned with the exponential growth of a small disturbance, but then attention turned to eddy life cycles. Edmon et al. (1980) described how, as a baroclinic disturbance grows, heat is transported polewards and the available potential energy of the mean flow is converted to eddy kinetic energy. However,

Responsible Editor: Pierre De Mey-Frémaux

Electronic supplementary material The online version of this article (https://doi.org/10.1007/s10236-018-1241-x) contains supplementary material, which is available to authorized users.

✉ Harry Leach
leach@liv.ac.uk

[1] Department of Earth, Ocean and Ecological Sciences, University of Liverpool, 4 Brownlow Street, Liverpool, L69 3GP, UK

[2] Alfred-Wegener-Institut, Helmholtz-Zentrum für Polar- und Meeresforschung, Postfach 12 01 61, D-27515 Bremerhaven, Germany

Published online: 20 December 2018

after passing maturity, the eddy decays and momentum is fed back *into* the jet and eddy kinetic energy returns to the kinetic energy of the mean flow. Work on the way in which eddies decay was done by Methven (1998) and Methven and Hoskins 1998, 1999); their calculations showed that, as an eddy forms, it winds in anomalies of potential vorticity, which eventually leads to an unstable situation and the eddy collapses releasing anomalies back into the mean flow. The interesting point is that once formed eddies do not simply decay by friction running them down, but rather collapse quickly. Chelton et al. (2011) have looked at the statistical properties of eddies based on the AVISO altimeter data and show that about 10% last 16 weeks or more, which corresponds to a half-life of about 5 weeks.

One of the processes which contribute to the evolution of eddies are fine-scale interleavings; these are thermohaline anomalies with a vertical scale of tens of metres, arising due to ageostrophic flow across fronts as part of the frontogenesis process (Joyce 1977; MacVean and Woods 1980; Woods et al. 1986). Frontogenesis is itself a process by which density and thermohaline gradients can sharpen on scales smaller than that of the eddies.

The Antarctic Circumpolar Current (ACC) is one of the most eddy-rich regions of the ocean; here the eddy transports across the ACC are particularly important for the global meridional overturning (Marshall and Speer 2012) and the subduction of anthropogenic CO_2 (Sallée et al. 2012; Bopp et al. 2015). Drake Passage, as one of the more accessible parts of the ACC, has received particular attention. Joyce et al. (1978) looked at the character of the interleavings near the Antarctic Polar Front (APF), and more recently, Thompson et al. (2007) looked at vertical diffusion on either side of the APF and reported that it is higher to the north than to the south. Earlier work on the genesis of cyclonic eddies from the APF in Drake Passage (Joyce et al. 1981; Peterson et al. 1982) largely focussed on the bulk properties, such as heat and freshwater content anomalies, as indeed have more recent studies (Swart et al. 2008; Kurczyn et al. 2013; Zhang et al. 2016). However, Joyce et al. (1981) do present a CTD section through a cyclonic eddy apparently freshly formed during the course of their experiment from the APF, and it appears to display greater interleaving on the edges. Adams et al. (2017) present sections from a towed system crossing the rim of a freshly formed cyclonic eddy in the Scotia Sea. The most complicated submesoscale structures are observed in the saddle region where the eddy is separating from its parent front. However, their sections do not extend to the centre of the eddy.

Armi and Zenk (1984) present a detailed study of lenses of high salinity water which were formed in the Mediterranean Outflow and then propagate southwestwards in the Canaries Basin. These "Meddies" are anticyclonic and have ages which may be measured in years, rather than months, and they too show stronger fine-scale variability around the edges than in the centre (Meunier et al. 2015). More generally, in recent years, submesoscale coherent vortices (SCV), first named by McWilliams (1985), have attracted much interest. These are generally anticyclonic subsurface features so that, in the northern hemisphere, they can have very negative relative vorticity, so that their Ertel potential vorticity can be negative. It seems that they are often generated by the interaction of boundary currents with topography (D'Asaro, 1988; Molemaker et al. 2015; Thomsen et al. 2016). Pietri and Karstensen (2018) describe the anatomy of a 7-month-old SCV formed near the coast of Mauretania and show that there is enhanced interleaving around the rim.

In this study, data from four eddies or mesoscale features were used, all from the Atlantic sector of the ACC. The ACC consists of a series of fronts (Gordon 1971; Gordon et al. 1977; Orsi et al. 1995; Sokolov and Rintoul 2009), or jets, which can become unstable and form eddies. All four cyclonic features studied contained lenses of cold Winter Water (WW) with temperature minima in the depth range 100–300 m and were trapped in the zone between the Antarctic Polar Front and the Southern Polar Front (Hibbert et al. 2009; Strass et al. 2017a). Close inspection of the character and structure of these four eddies combined with estimates of their ages from altimeter data suggests how eddies might evolve after they have formed. In this paper, we will consider both the mesoscale structure of the eddies, in terms of maps, sections and θS diagrams, and also the distribution of measures of fine-scale variability. By looking at both the mesoscale and fine-scale properties of the eddies, we can gain some insight into how the properties of water masses trapped in eddies might be modified before rerelease into the general flow. It should be stressed though, that, while we have used parameters derived from individual CTD profiles as measures of fine-scale variability, we are nevertheless of the opinion that, so far as the mesoscale is concerned, lateral stirring by submesoscale processes and then mixing are more important than diapycnic processes alone (see, Hibbert et al. 2009; Smith and Ferrari 2009; Leach et al. 2011).

In addition to controlling the exchange of physical properties across the ACC, eddies are involved in the interplay of physical, chemical and biological processes which limit primary productivity, and hence CO_2 drawdown, in the Southern Ocean. The supply of silica or iron, limitation by light and grazing pressure are all held to be contributary factors by a variety of authors (see for example, Martin 1990; Moore and Abbott 2000, 2002; Ito et al. 2005; Behrenfeld 2010; Hoppe et al. 2017), but the horizontal and vertical rates of exchange will be controlled by the eddy field (Strass et al. 2002; Jones et al. 2017).

This study is largely based on data obtained by vertical CTD casts; although other data were collected during some of the surveys, it was by no means so systematic and uniform as the basic CTD cast data. Vessel-mounted ADCP data are available for all the surveys and shown in Hibbert et al. (2009) and Strass et al. (2017a), but generally just show the same eddy structure as the hydrography and so have not been repeated here. This study makes use of a variety of parameters from the upper thermocline, starting below the surface layer at a 100-m depth and extending to the potential temperature maximum of the Upper Circumpolar Deep Water (UCDW) at about 500 m depth and encompassing the WW potential temperature minimum at about a 150-m depth. At the low temperatures in question, the nonlinearity of the equation of state means that density depends almost solely on salinity, so that temperature can be regarded as a passive tracer.

In this paper, we have adopted the convention that the units of temperature (relative to the freezing point of pure water) are ^{o}C while units of temperature difference are K. At the low temperatures encountered temperatures and temperature differences can be numerically similar and this convention helps distinguish between them.

2 Data

Both the cruises, from which the data were used in this study, were primarily biogeochemical in their aims, designed to study either artificially stimulated or naturally occurring phytoplankton blooms so that the work reported here is essentially a by-product using data not designed for the purpose.

The track of *Polarstern* Cruise ANTXXI/3—"EIFEX"—leaving from Cape Town on 21st January 2004 (Smetacek 2005) and arriving back in Cape Town on 25th March 2004 is shown in Fig. 1. The purpose of this cruise was to conduct an iron fertilisation experiment in the ACC. The reason for using an eddy was that the water fertilised with iron sulphate would be trapped and relatively easy to follow (Strass et al. 2005). The first eddy (Eddy 1) selected on the basis of altimeter data was at about 50^{o} S, 18^{o} E. This eddy was surveyed during a period of 7 days between 25th January and 1st February 2004 by CTD/Rosette casts along five equally spaced meridional sections. Along the westernmost section, 17^{o} E, the station spacing was 5 mi (9 km), and along the other 4 (17^{o} 40', 18^{o} 20', 19^{o} 00' and 19^{o} 40' E), it was 12 mi (22 km); the sections were completed systematically working from west to east. Investigation revealed that the initial chlorophyll concentration was too low for the fertilisation experiment and so this eddy was rejected, but not before a useful set of physical data had been obtained. Instead, a second eddy (Eddy 2), at about

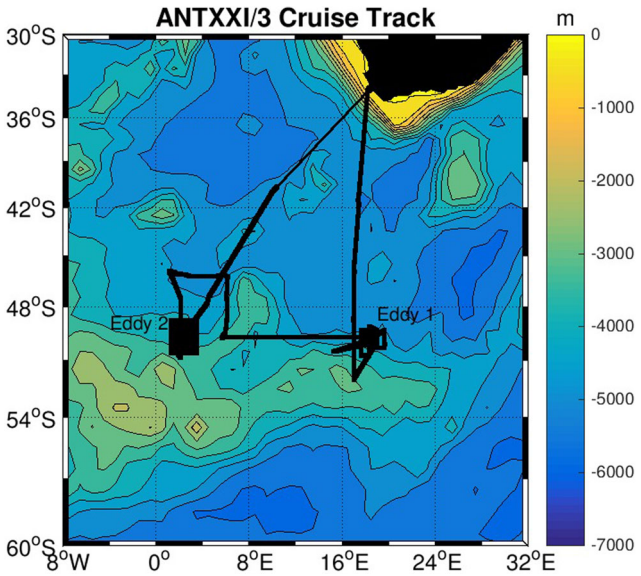

Fig. 1 Track of *Polarstern* Cruise ANTXXI/3—"EIFEX"—leaving from Cape Town on 21st January 2004 and arriving back in Cape Town on 25th March 2004

49^{o} S, 2^{o} E was selected for the experiment and was ultimately occupied for a period of 40 days. Altogether, this eddy was investigated during the period 8th February to 20th March 2004; however, the data for the initial CTD/Rosette survey were collected during a period of 6 days between 14th and 20th February. The stations were evenly spaced 12 mi (22 km) apart meridionally and zonally, or 12' latitude and about 18.6' of longitude, with ten stations along each of eight equally spaced meridional sections between 1^{o} 19' and 3^{o} 29' E. The sections were collected systematically from west to east. This second eddy was the one from which Smetacek et al. (2012) reported on the massive export event at the end of the iron-fertilised bloom. Hibbert et al. (2009) used the evolution of the core temperature of this eddy to draw conclusions about the rate of mixing of water within the eddy and compared the θS relationships to support their ideas about the homogenisation of properties within the eddy over time.

The track of *Polarstern* Cruise ANTXXVIII/3—"Eddy-Pump"—leaving from Cape Town on 7th January 2012 and arriving in Punta Arenas on 11th March 2012 (Wolf-Gladrow 2013) is shown in Fig. 2. The purpose of this cruise was to look at naturally occurring late-season phytoplankton blooms in the ACC; most of the biogeochemical results of this cruise are published in Strass et al. (2017b). Unusually, this time the Atlantic Sector of the Southern Ocean seemed devoid of any useful isolated eddies, so that initially a meridional section across the ACC was made at 10^{o} E. After that, two mesoscale features were investigated. The first was on the west side of the

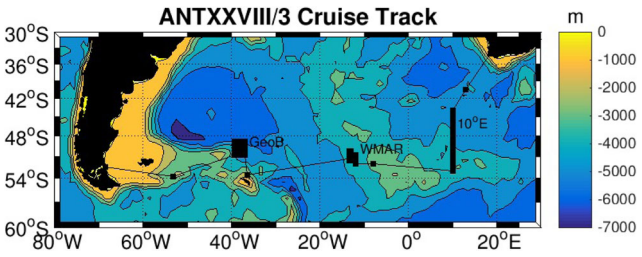

Fig. 2 Track of *Polarstern* Cruise ANTXXVIII/3—"Eddy-Pump"–leaving from Cape Town on 7th January 2012 and arriving in Punta Arenas on 11th March 2012

Mid-Atlantic Ridge at about 51^o S, 13^o W (the West Mid-Atlantic Ridge Survey, WMAR) and the second was in the Georgia Basin at about 50^o S, 38^o W (the Georgia Basin Survey, GeoB). The first survey (WMAR), conducted between 29th January and 19th February 2012, consisted of a grid of 5 × 5 CTD stations with 12 mi (22 km) spacing. The stations at the corners and centres of the sides as well as the Central Station were to full depth, while the intermediate stations were to 500 m. There was an extension of six stations to the northwest to 1500 m depth. The Central Station at 51^o 12' S, 12^o 40' W, was repeated seven times and a few others twice. A station at 52^o S, 12^o W and two in the NW extension region, all completed before the survey began, have been included in the mapping. The second survey (GeoB), conducted between 24th February and 3rd March 2012, was centred on 50^o 48' S, 38^o 12' W, and consisted of five meridional sections of six CTD stations 24 mi (44 km) apart, both east-west and north-south, to 1000 m depth.

During both cruises, hydrographic data were obtained using a Sea-Bird Electronics SBE 911plus Conductivity, Temperature and Depth (CTD) sonde. The sensors were calibrated at the factory before and after the cruise, the temperature sensors to a final error of approximately 0.001 ^{o}C and the pressure sensor to 0.01%. The CTD was mounted in a multi-bottle water sampler type Sea-Bird SBE 32 Carousel holding 24 12-litre bottles, though in ANTXXVIII/3 two bottles were replaced by an RDI LADCP (Strass et al. 2001, 2017a). Salinities derived from the CTD measurements were later recalibrated by comparison with salinity samples taken from the water bottles, which were analyzed using a laboratory salinometer to an uncertainty generally below 0.001 units on the practical salinity scale, adjusted to IAPSO Standard Seawater (Smetacek 2005; Wolf-Gladrow 2013).

For some of the eddy surveys, physical data from instruments other than the CTD were available, such as the free-falling MSS turbulence sonde in EIFEX Eddy 2 (Cisewski et al. 2008) and in the Eddy-Pump WMAR (Strass et al. 2017a). However, the spatial coverage of the structures was not as good as the CTD stations. During the Eddy-Pump Cruise, some lowered ADCP data were collected, but again not so systematically as to be useful; in addition, there was a clock offset, which was not exactly known (Strass et al. 2017a). Only the CTD data provided a consistent dataset with the best coverage of the four structures described here, so it was decided to restrict this paper to these data. Hull-mounted ADCP data were collected throughout the cruises, but generally showed the same eddy structures as the CTD data, so that for the sake of brevity these have been omitted, but are available in Hibbert et al. (2009) for the ANTXXI/3 EIFEX Cruise and Strass et al. (2017a) for the ANTXXVIII/3 Eddy-Pump Cruise.

For comparison with the in situ hydrographic data, the merged altimetric data offered on the Aviso website (http://www.aviso.altimetry.fr/en/data.html, now hosted by marine.copernicus.eu) were used. Extracts of the data for the region of interest were provided in user-friendly form by colleagues at the National Oceanography Centre in Liverpool.

3 Methods

Three parameters have been used to characterise the mesoscale structures. Firstly, the WW potential temperature minimum, $\theta_{\min}$, at each station was determined. Secondly, the mean potential density, $\overline{\sigma_\theta}$ was calculated by taking the average for the depth range 100–480 m, except for EIFEX Eddy 1 where the lower depth had to be limited to 390 m as some casts on the westernmost section barely reached 400 m. Thirdly, the layer-thickness contribution to the potential vorticity for the depth range was calculated using:

$$q = -\frac{f}{\overline{\rho}}\frac{\Delta\sigma_\theta}{\Delta z} \tag{1}$$

where f is the Coriolis parameter, $\overline{\rho}$ is the mean density of the layer, $\Delta\sigma_\theta$ the density difference over the depth range Δz, 100–480 (or 390) m. While this is not the whole Ertel potential vorticity, it should be the major contribution on the mesoscale (Fischer et al. 1989) and adequate for locating the eddy. The reason for standardising on these parameters for this depth range was that some of the CTD casts were only made to 500 m and so may not have reliably quite reached the UCDW $\theta_{\max}$, and it was desired to make use of as many stations as possible to enhance statistical significance.

To characterise the fine-scale variability, two parameters were used. The CTD data from all surveys showed a rich and varied pattern of interleaving structures and ways were sought in which this might be quantified. The profiles of potential temperature showed considerable variability both in the shape of the WW potential temperature minimum

itself, and also in the character of the profile between this temperature minimum, $\theta_{\min}$, at about a 150-m depth and the UCDW $\theta_{\max}$ at about a 500-m depth. In this depth range, there was considerable fluctuation about what might be considered to be a "mean profile". To characterise this variability, the idea of looking at the root mean square variance about a smooth curve was tried. Finding a mathematical curve to approximate the $\theta_{\min}$ itself proved very challenging, and eventually, a fourth-order polynomial

$$\theta_i = a_0 + a_1 z_i + a_2 z_i^2 + a_3 z_i^3 + a_4 z_i^4 + \epsilon_i \tag{2}$$

was fitted to the potential temperature in the depth range between $\theta_{\min}$ and 480 m (or 390 m for EIFEX Eddy 1) minimising $\overline{\epsilon_i^2}$ in the usual way, so that the smoothed or model potential temperature was as follows:

$$\hat{\theta} = a_0 + a_1 z + a_2 z^2 + a_3 z^3 + a_4 z^4 \tag{3}$$

and then the root mean square fluctuation about this curve was calculated:

$$\theta_{\text{rms}} = \sqrt{\frac{1}{n}\Sigma\left(\theta_i - \hat{\theta}(z_i)\right)^2} \tag{4}$$

As a way of characterising turbulent overturns the vertical diffusivity based on the Thorpe scale (Thorpe 1977), K_T, was calculated using σ_θ for the depth range 100–480 (or 390) m. The Thorpe-scale itself, L_T, is the root mean square displacement of water particles when a potential density σ_θ profile is monotonised by sorting:

$$L_T = \sqrt{\frac{1}{n}\Sigma\left(z_i^{\text{sorted}} - z_i^{\text{unsorted}}\right)^2} \tag{5}$$

and

$$K_T = 0.2 N L_T^2 \tag{6}$$

where N is the Brunt-Väisälä frequency.

Because of the nonlinearity of the equation of state, at the low temperatures encountered in the ACC, temperature has virtually no effect on density which is determined almost entirely by salinity, so that θ_{rms} and K_T should be reasonably independent one of another; using two relatively independent measures of fine-scale variability should gives more confidence in the results.

Throughout this paper, contoured maps and sections are used to display the structures of the mesoscale features described. Because of the different ranges of values in the different structures observed, it is not possible to use one colour scheme for the same parameter in all diagrams and be able to see the structures clearly. Therefore, we have not used a uniform colouring system; since the principal purpose of the paper is to compare structures, rather than absolute values of the parameters, this should not be too much of a hinderance.

4 Results

In this section, we will consider our four mesoscale structures in order of apparent age starting with the youngest, EIFEX Eddy 1, followed by the Eddy-Pump Georgia Basin Survey, then EIFEX Eddy 2 and finally the Eddy-Pump West Mid-Atlantic Ridge Survey.

4.1 EIFEX Eddy 1

According to the Aviso Data (http://www.aviso.altimetry.fr/en/data.html), this feature is only 2 to 3 weeks old, and so is still very young (Hibbert et al. 2009) (see Supplementary Material 1_EIFEX_Eddy_1.mov).

Maps of mesoscale and fine-scale quantities are shown in Fig. 3. The WW potential temperature minimum, $\theta_{\min}$, (a) stretches from the SW corner into the centre of the survey area with a coldest temperature of about 0.4 ^{o}C. The mean density, $\overline{\sigma_\theta}$, shows the reverse with a maximum where the water is coldest. The potential vorticity, q, (b) shows a minimum in the centre of the survey area, corresponding to the coldest water, with less negative values surrounding it; in the Southern Hemisphere potential vorticity is negative and more negative potential vorticity represents a cyclonic feature with negative vorticity and a cold core. The root-mean square potential temperature fluctuations, θ_{rms} (c) shows maxima where the water is coldest. The Thorpe-scale-based diffusivity K_T (d) shows larger values in the colder water. K_T has values in the range 1×10^{-4} to 1×10^{-3} $m^2\ s^{-1}$.

Plots of parameters for the ANTXXI/3 EIFEX Eddy 1 Survey as a function of the distance from the eddy centre at 49.75^o S, 18.30^o E including the regression line are shown in Fig. 4. The potential temperature at the WW potential temperature minimum, $\theta_{\min}$ in ^{o}C, (a) shows a positive correlation with distance (R = 0.360, p = 0.005), while the potential vorticity calculated for the depth range 100–390 m in rad s^{-1} Gm^{-1} (b) shows no significant correlation with distance from the eddy centre (R = 0.037, p = 0.778). Both the root mean square variability of potential temperature θ_{rms} in K (c) (R = − 0.134, p = 0.328) and the vertical diffusivity based on the Thorpe-scale K_T in $m^2\ s^{-1}$ (d) (R =− 0.250, p = 0.054) show weak decreases with distance from the centre.

Meridional sections of potential temperature and density along 18^o 20' E through the eddy centre are shown in Fig. 5. The lens of cold WW can be seen in the latitude range 49.5 to 50.0 ^{o}S and depth range 100 to 300 m. Indeed two separate cores of the coldest water can be seen, one at 49.6^o S and a 250-m depth, and the other at 49.75^o S and about a 175-m depth. The isopycnals show a distinct doming centred under the cold WW lens. The nonlinearity of the equation of state means that, at

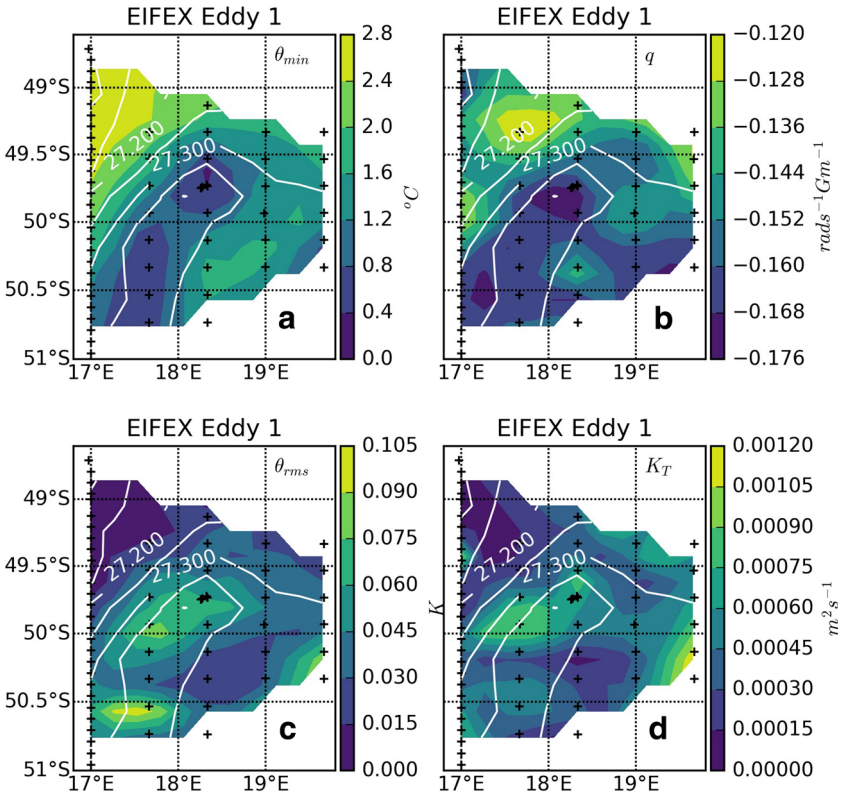

Fig. 3 Maps of parameters for the ANTXXI/3 EIFEX Eddy 1 Survey overlain with mean potential density $\overline{\sigma_\theta}$ for the upper thermocline depth range 100–390 m with a contour interval of 0.05 kg m^{-3} showing a maximum in the middle of the area: **a** potential temperature at the Winter Water potential temperature minimum, $\theta_{\min}$ in ^{o}C, **b** potential vorticity calculated for the depth range 100–390m in rad s^{-1} Gm^{-1}, **c** the root mean square variability of potential temperature in pressure coordinates $\theta_{\rm rms}$ in K, **d** the vertical diffusivity based on the Thorpe-scale K_T in $m^2\ s^{-1}$

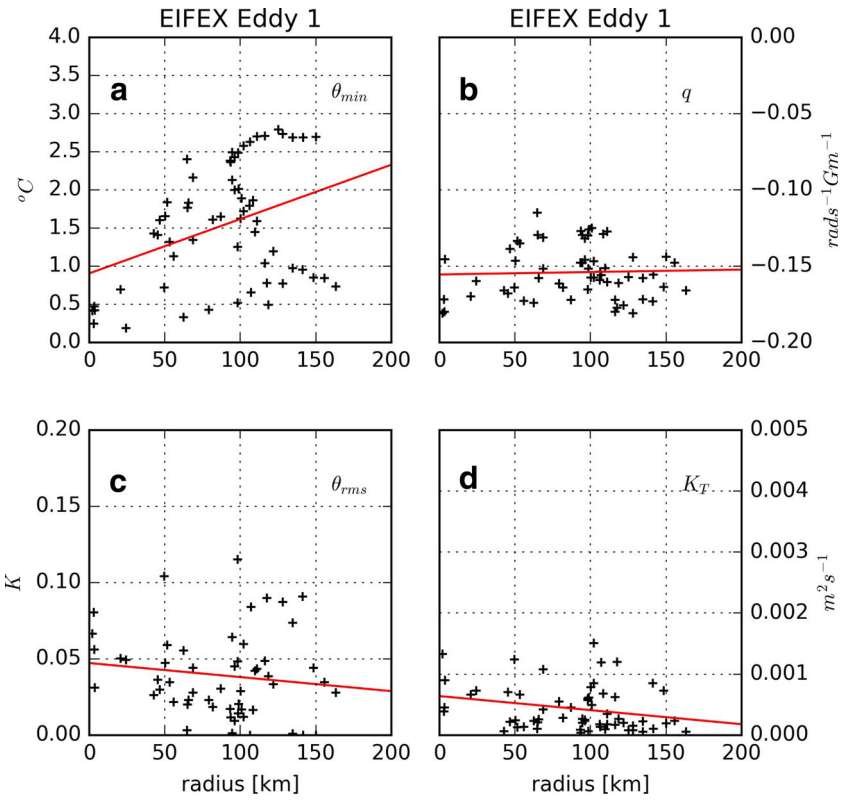

Fig. 4 Plots of parameters for the ANTXXI/3 EIFEX Eddy 1 Survey as a function of the distance from the eddy centre at 49.75^o S, 18.30^o E including the regression line: **a** potential temperature at the Winter Water potential temperature minimum, $\theta_{\min}$ in ^{o}C ($R = 0.360$, $p = 0.005$), **b** potential vorticity calculated for the depth range 100–390 m in rad s^{-1} Gm^{-1} ($R = 0.037$, $p = 0.778$), **c** the root mean square variability of potential temperature in pressure coordinates $\theta_{\rm rms}$ in K ($R = -0.134$, $p = 0.328$), **d** the vertical diffusivity based on the Thorpe-scale K_T in $m^2\ s^{-1}$ ($R = -0.250$, $p = 0.054$)

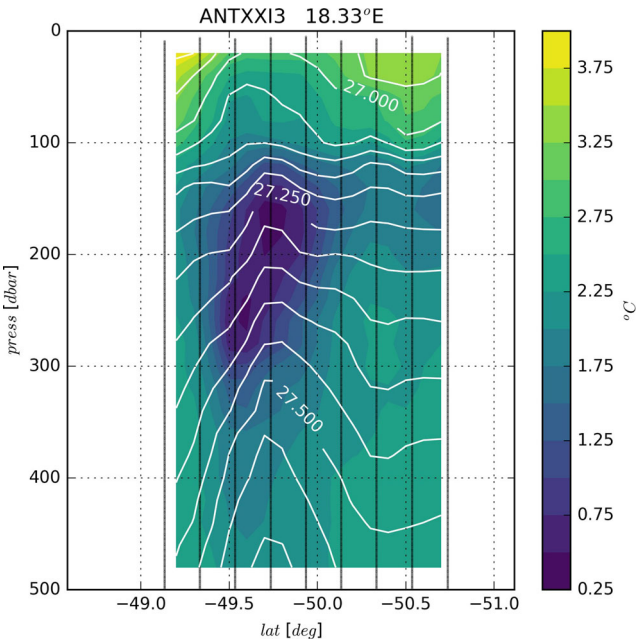

Fig. 5 Meridional section through ANTXXI/3 EIFEX Eddy 1 along 18^o 20' E showing potential temperature θ and overlain with density σ_θ in the top 500 m in white. Note the lens of cold Winter Water and the corresponding domed isopycnals centred at 49.75^o S. For scale 1^o of latitude corresponds to 111 km. The station positions are marked by thin black lines

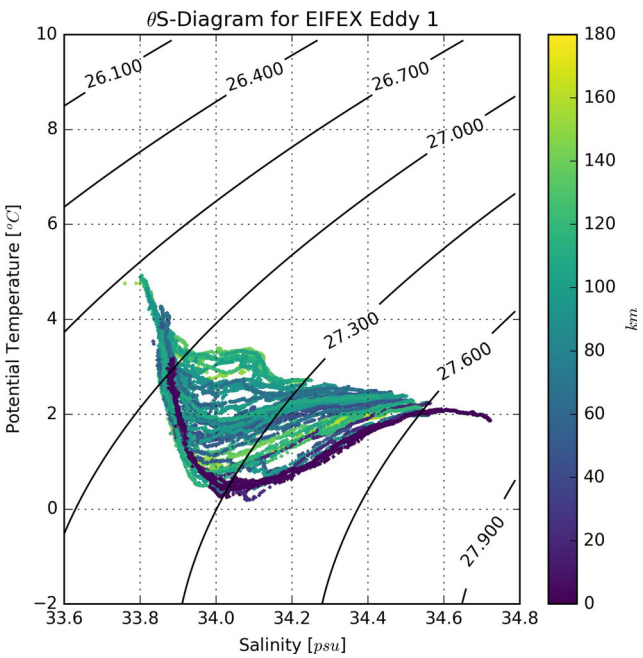

Fig. 6 Potential temperature-salinity, θS, diagram for the ANTXXI/3 EIFEX Eddy 1 Survey. Contours of potential density, σ_θ, are shown in black. Notice the broad range of local water masses present, in particular the wide variety of Winter Water θ minima from ca. 0.5 ^{o}C to above 2.0 ^{o}C. The profiles are coloured by the distance from the eddy centre at 49.75^o S, 18.30^o E

the temperatures encountered, density is determined almost entirely by salinity and temperature is effectively a passive tracer. Because the isohalines and isopycnals look virtually identical, we have not included salinity sections.

In the θS diagram, Fig. 6, a wide variety of profiles can be seen with potential temperature minima ranging from about 0.5 ^{o}C up to about 3.0 ^{o}C. The profiles at the centre of the eddy are shown in dark blue, but the variety of shades, with lighter ones further from the centre, shows that the eddy core is relatively inhomogeneous.

4.2 Eddy-Pump Georgia Basin Survey (EP GeoB)

Looking at the Aviso Data (http://www.aviso.altimetry.fr/en/data.html) sequence in the period leading up to the survey, it can be seen that cyclonic features are being repeatedly formed in the topographically steered flow to the west of the survey area and being injected into this area from the west. In this particular case, the eddy-like feature becomes apparent about the middle of January and our survey was at the end of February and beginning of March, so that the eddy when investigated was perhaps 6 weeks old (see Supplementary Material 2_Georgia_Basin.mov).

The WW $\theta_{\min}$ distribution in the Georgia Basin Survey (Fig. 7a) shows that the area is dominated by a large cold core structure with warmer water along the northern and eastern margins, though here there seem to be poorly resolved smaller scale structures. The occurrence of broad topographically controlled meanders in this region is well-documented (Peterson and Whitworth 1989; Orsi et al. 1995); the Aviso sequence suggests that they continually reform in the same position. The coldest waters have a $\theta_{\min}$ less than 0.4 ^{o}C, while the least cold $\theta_{\min}$ in the NE corner is about 2.4 ^{o}C. The mean density $\overline{\sigma_\theta}$ shows denser water dominating the centre, west and south of the area with lighter water in the NW and NE corners and on the eastern boundary. The potential vorticity, q (b), also shows the same structure with more negative values in the centre, west and south and less negative values in the NW, NE and on the eastern boundary. The horizontal distribution of q indicates that the cold and dense cores are associated with cyclonic circulation which dominates the area surveyed with smaller meanders around the northern and eastern rim.

The variability of potential temperature as measured by θ_{rms} (c) shows larger values south and east of the centre of the eddy. The vertical diffusivity based on the Thorpe-scale, K_T (d), has values in the range 1×10^{-4} to 3×10^{-3} m^2 s^{-1} with isolated maxima both in the centre and to the east of the centre of the eddy.

Figure 8 shows parameters for the ANTXXVIII/3 Eddy-Pump Georgia Basin Survey as a function of the distance from the eddy centre at 49.80^o S, 38.75^o W including the regression line. Potential temperature at the Winter Water

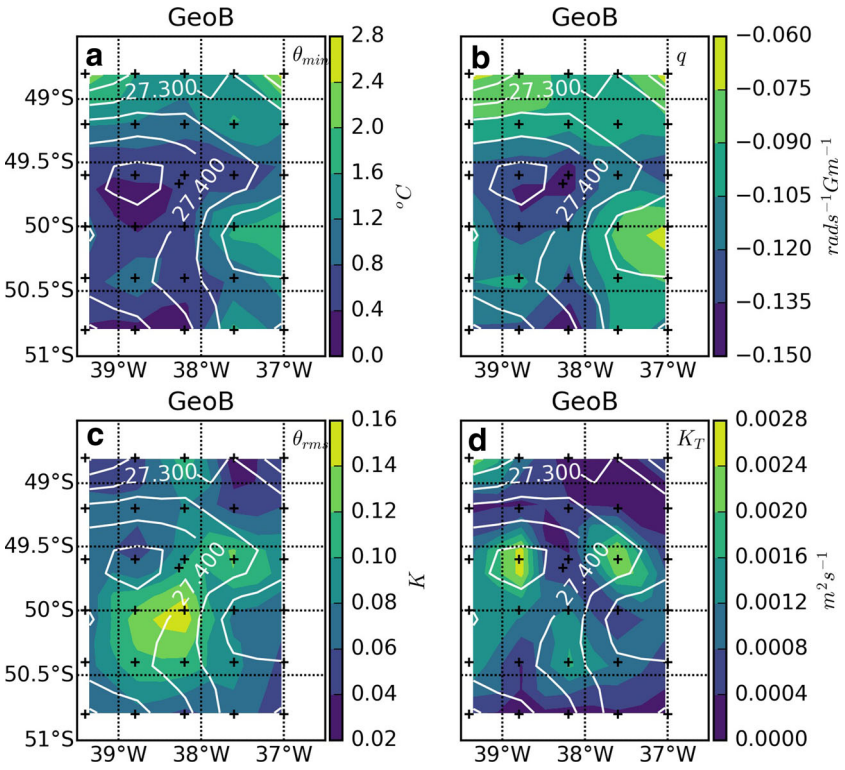

Fig. 7 Maps of parameters for the ANTXXVIII/3 Eddy-Pump Georgia Basin Survey overlain with the mean potential density $\overline{\sigma_\theta}$ for the upper thermocline depth range 100–480 m with a contour interval of 0.05 kg m^{-3}; the closed contour is a density maximum: **a** potential temperature at the Winter Water potential temperature minimum, $\theta_{\min}$ in ^{o}C, **b** potential vorticity calculated for the depth range 100–480 m in rad s^{-1} Gm^{-1}, **c** the root mean square variability of potential temperature in pressure coordinates θ_{rms} in K, **d** the vertical diffusivity based on the Thorpe-scale K_T in $m^2\ s^{-1}$

potential temperature minimum, $\theta_{\min}$ in ^{o}C (a) ($R = 0.585$, $p = 0.0004$) and potential vorticity calculated for the depth range 100–480 m in rad s^{-1} Gm^{-1} (b) ($R = 0.510, p = 0.003$) both show significant correlations with distance from the eddy centre. The root mean square variability of potential temperature θ_{rms} in K (c) ($R = -0.337$, $p = 0.060$) and the

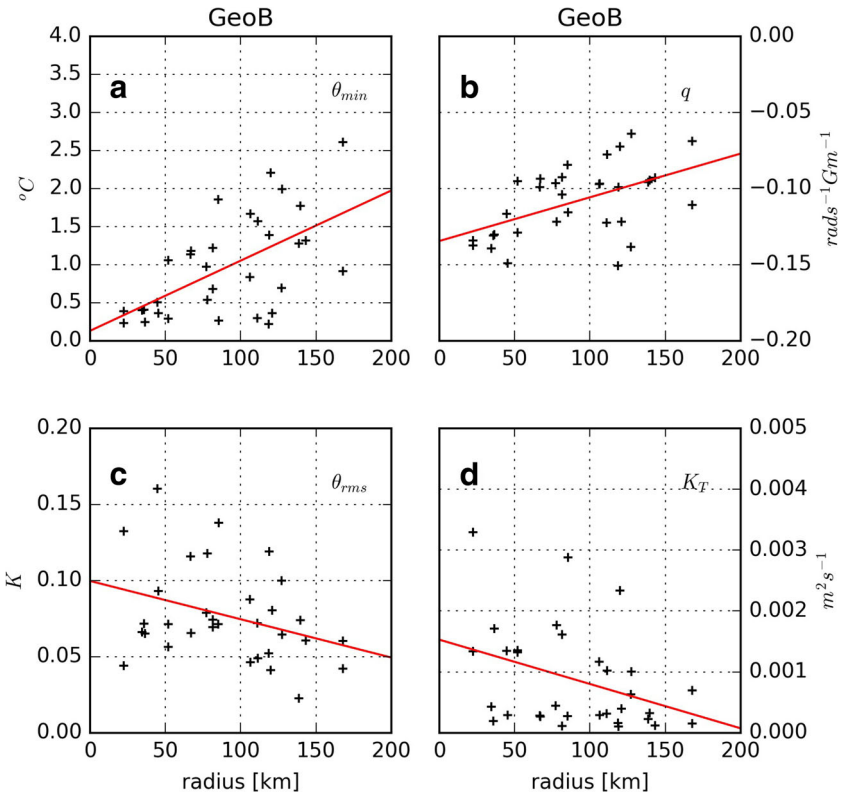

Fig. 8 Plots of parameters for the ANTXXVIII/3 Eddy-Pump Georgia Basin Survey as a function of the distance from the eddy centre at 49.80^o S, 38.75^o W including the regression line: **a** potential temperature at the Winter Water potential temperature minimum, $\theta_{\min}$ in ^{o}C ($R = 0.585$, $p = 0.0004$), **b** potential vorticity calculated for the depth range 100–480 m in rad s^{-1} Gm^{-1} ($R = 0.510$, $p = 0.003$), **c** the root mean square variability of potential temperature in pressure coordinates θ_{rms} in K ($R = -0.337$, $p = 0.060$), **d** the vertical diffusivity based on the Thorpe-scale K_T in $m^2\ s^{-1}$ ($R = -0.362$, $p = 0.042$)

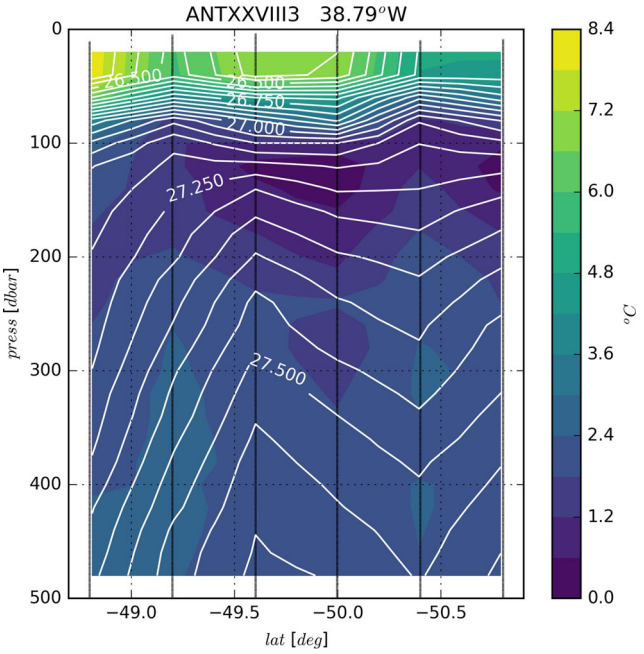

Fig. 9 Meridional section through the ANTXXVIII/3 Eddy-Pump Georgia Basin Eddy along 38^o 48' W, through the $\theta_{\min}$ minimum and the $\overline{\sigma_\theta}$ maximum, showing potential temperature θ and overlain with density σ_θ in the top 500 m in white. Note the lens of cold Winter Water and the corresponding domed isopycnals centred between 49.5 and 50.0^{o}S. For scale 1^o of latitude corresponds to 111 km. The station positions are marked by thin black lines

vertical diffusivity based on the Thorpe-scale K_T in $m^2\ s^{-1}$ (d) ($R = -0.362$, $p = 0.042$) both show significant negative correlations with distance from the eddy centre.

In Fig. 9, the section of potential temperature and density along 38^o 48' W, through the $\theta_{\min}$ minimum and the $\overline{\sigma_\theta}$ maximum, is shown. The lens of cold WW can be seen centred between 49.5 and 50.0^o S with up-domed isopycnals beneath, but a flattening or M-shaped structure above.

The θS diagram in Fig. 10 shows a broad range of profiles with WW $\theta_{\min}$ ranging from about 0.2 ^{o}C up to about 2.0 ^{o}C with incipient salinity minima at about 34.1 and 2–3 ^{o}C indicating the proximity of the Sub-Antarctic Front at which the Antarctic Intermediate Water subducts. The profiles at the centre of the eddy are shown in dark blue, and, with some exceptions, the profiles further away from the centre, shown in lighter shades, are warmer and saltier.

4.3 EIFEX Eddy 2

This feature is reckoned to be about 6 months old by Hibbert et al. (2009) based on the Aviso Data (http://www.aviso.altimetry.fr/en/data.html)(see Supplementary Material 3_EIFEX_Eddy_2.mov).

All three mesoscale parameters, $\theta_{\min}$, $\overline{\sigma_\theta}$ and q, Fig. 11a, b, show a closed cold core eddy centred in the north of the survey area. The coldest temperature in the WW core is about 1.0 ^{o}C, which is rather warmer than in the two previous examples. Hibbert et al. (2009) reported that mixing processes within the eddy increased the temperature by 0.15 K over a period of 40 days, so that a warming of 0.6 K, compared to the EIFEX Eddy 1 core temperature of 0.4 ^{o}C could be accomplished in 160 days, or about 5 months. The cold core corresponds to a density maximum and potential vorticity minimum.

The fine-scale parameters for EIFEX Eddy 2, $\theta_{\rm rms}$ Fig. 11c, and K_T (d), show generally small values in the eddy centre and a series of isolated larger values, mostly dotted around the edge. K_T has values in the range 1×10^{-4} to $4 \times 10^{-3}\ m^2\ s^{-1}$.

Plots of parameters for the ANTXXI/3 EIFEX Eddy 2 Survey as a function of the distance from the eddy centre at 49.25^o S, 2.25^o E including the regression line are shown in Fig. 12. Potential temperature at the WW potential temperature minimum, $\theta_{\min}$ in ^{o}C (a) ($R = 0.243$, $p = 0.030$) and the potential vorticity calculated for the depth range 100–480 m in rad s^{-1} Gm^{-1} (b) ($R = 0.246$, $p = 0.028$) show significantly positive correlations with distance from the

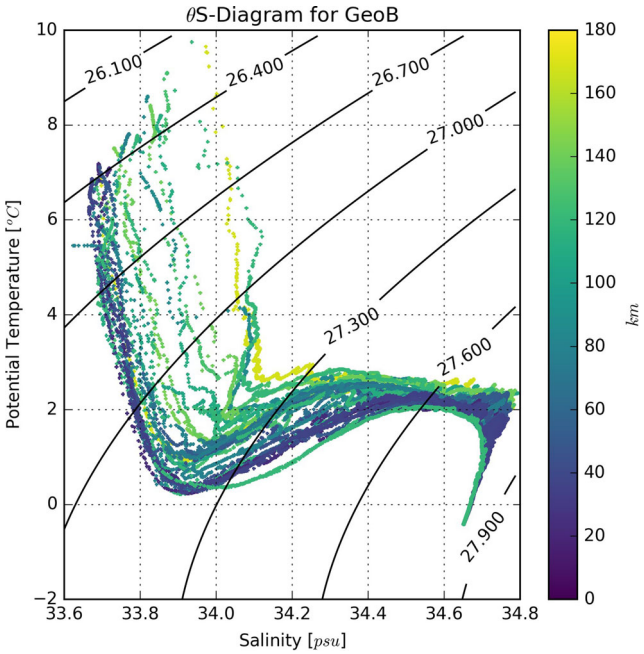

Fig. 10 Potential temperature-salinity, θS, diagram for the ANTXXVIII/3 Eddy-Pump Georgia Basin Eddy Survey. Contours of potential density, σ_θ, are shown in black. Notice the broad range of local water masses present, in particular the wide variety of Winter Water θ minima from ca. 0.2 ^{o}C to above 2.0 ^{o}C. Notice also the incipient salinity minima in the range 34.0 to 34.1. The profiles are coloured by the distance from the eddy centre at 49.80^o S, 38.75^o W

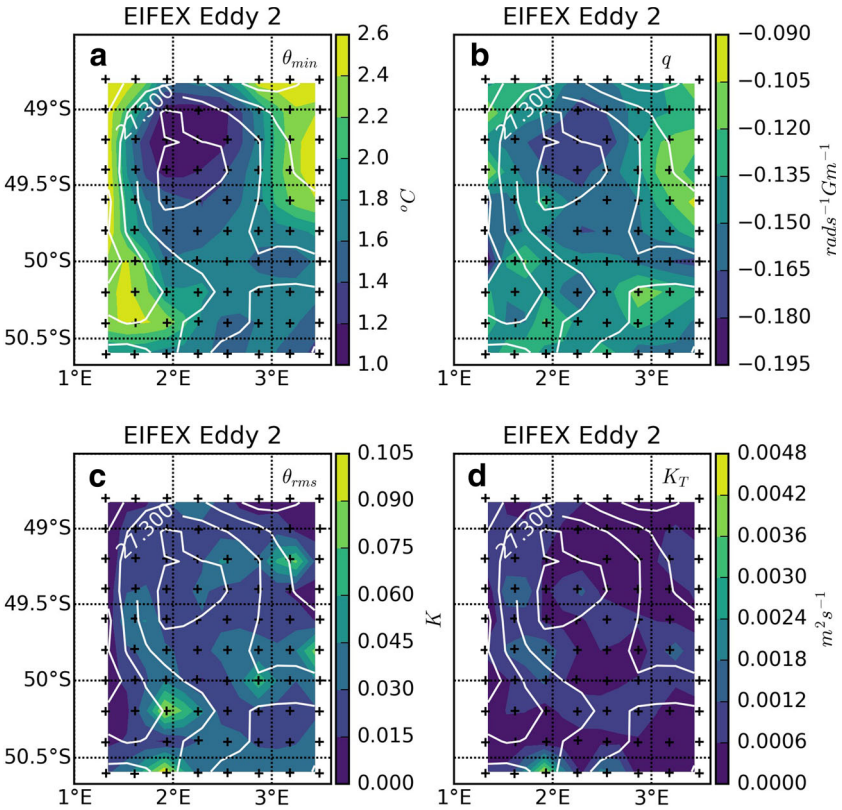

Fig. 11 Maps of parameters for the ANTXXI/3 EIFEX Eddy 2 Survey overlain with the mean potential density $\overline{\sigma_\theta}$ for the upper thermocline depth range 100–480 m with a contour interval of 0.05 kg m^{-3}; the closed contour is a density maximum: **a** potential temperature at the Winter Water potential temperature minimum, $\theta_{\min}$ in ^{o}C, **b** potential vorticity calculated for the depth range 100–480 m in rad s^{-1} Gm^{-1}, **c** the root mean square variability of potential temperature in pressure coordinates $\theta_{\rm rms}$ in K, **d** the vertical diffusivity based on the Thorpe-scale K_T in $m^2\ s^{-1}$

eddy centre. The root mean square variability of potential temperature in pressure coordinates $\theta_{\rm rms}$ in K (c) ($R = 0.162$, $p = 0.152$) and the vertical diffusivity based on the Thorpe-scale K_T in $m^2\ s^{-1}$ (d) ($R = 0.123$, $p = 0.278$) show weak positive correlations with distance from the eddy centre.

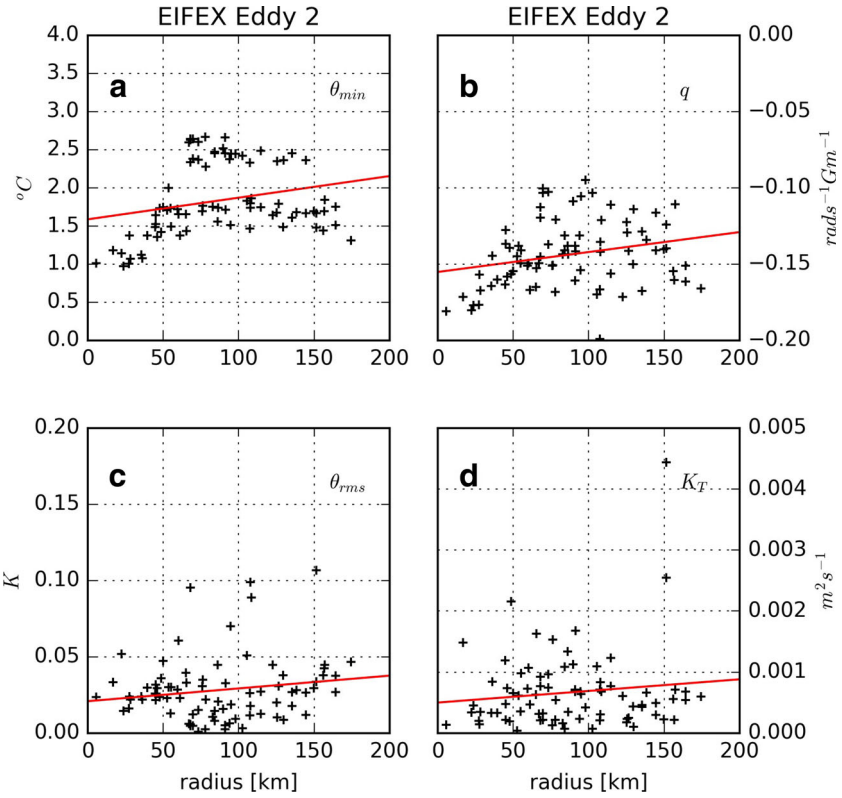

Fig. 12 Plots of parameters for the ANTXXI/3 EIFEX Eddy 2 Survey as a function of the distance from the eddy centre at 49.25^o S, 2.25^o E including the regression line: **a** potential temperature at the Winter Water potential temperature minimum, $\theta_{\min}$ in ^{o}C ($R = 0.243$, $p = 0.030$), **b** potential vorticity calculated for the depth range 100–480 m in rad s^{-1} Gm^{-1} ($R = 0.246$, $p = 0.028$), **c** the root mean square variability of potential temperature in pressure coordinates $\theta_{\rm rms}$ in K ($R = 0.162$, $p = 0.152$), **d** the vertical diffusivity based on the Thorpe-scale K_T in $m^2\ s^{-1}$ ($R = 0.123$, $p = 0.278$)

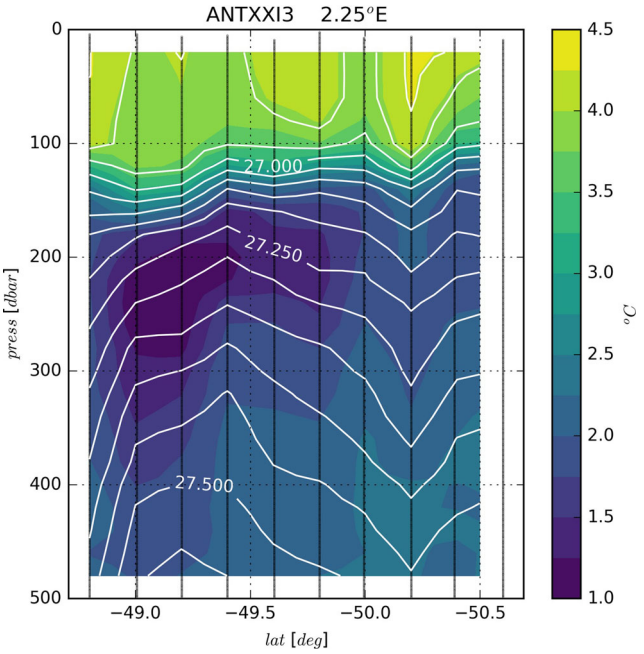

Fig. 13 Meridional section through ANTXXI/3 EIFEX Eddy 2 along 2^o 15' E showing potential temperature θ and overlain with density σ_θ in the top 500 m in white. Note the lens of cold Winter Water thickest at about 49.2^o S and how the isopycnals there are less sharply domed. For scale 1^o of latitude corresponds to 111 km. The station positions are marked by thin black lines

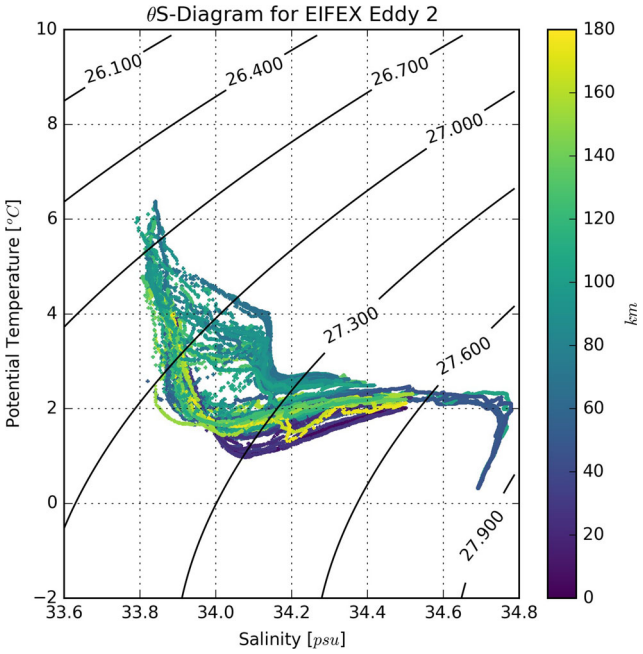

Fig. 14 Potential temperature-salinity, θS, diagram for the ANTXXI/3 EIFEX Eddy 2 Survey. Contours of potential density, σ_θ, are shown in black. Notice the bundling of local water masses, in particular the Winter Water θ minima below 2.0 ^{o}C of the water within the eddy and the distinct group with θ minima above 2.0 ^{o}C outside the eddy core. The profiles are coloured by the distance from the eddy centre at 49.25^o S, 2.25^o E

The section along 2^o15' E approximately through the eddy centre, Fig. 13, shows the thickest part of the WW $\theta_{\min}$ in the latitude range 49.0–49.2^o S. Though the isopycnals show a generally broad dome shape, in this range there are signs of a flattening of the isopycnals in the upper water column.

The θS diagram, Fig. 14, shows a more ordered relationship than in the previous cases, with a small set of WW $\theta_{\min}$ at about 1 ^{o}C, more in the range 1.5–2.0 ^{o}C and then a separate group at about 2.5 ^{o}C and salinity 34.10–34.15 representing the water immediately outside the eddy. The dark-blue curves represent the profiles near the centre of the eddy. The profiles with minima about 1.5 ^{o}C are paler indicating that they are at some distance away from the eddy centre which is towards the north of the survey area; these profiles come from the col region in the SE where the eddy is still separating from its parental front.

4.4 Eddy-Pump West Mid-Atlantic Ridge Survey (EP WMAR)

Looking at the Aviso Data (http://www.aviso.altimetry.fr/en/data.html), it can be seen that an anticyclonic feature grows over several weeks in the west of our survey area and reaches a maximum intensity in November 2011 centred at 51^o 40' S, 12^o 50' W. From then on, it gradually decays and can still be seen on the western boundary of our in situ survey in February 2012 (Fig. 15) as a southward meander. To the east of this anticyclone, there are persistent weak cyclonic features, northward meanders, which encroach into the area as the anticyclone weakens reinvigorating the cyclonic feature in the NW at the end of December/beginning of January, but the feature we observed in situ in February is hard to distinguish at all (see, Supplementary Material 4_West_MAR.mov).

The hydrographic structure in this survey can be typified by the minimum potential temperature of the WW, $\theta_{\min}$, shown in Fig. 15a. The main part of the survey area shows a warmer, southward, poleward meander ("ridge") in the west and a cooler, northward, equatorward meander ("trough") in the east with the survey covering virtually one zonal wavelength. Within the trough is a closed $\theta_{\min}$ contour with a value less than 1.3 ^{o}C. The northwest extension has the least cold water with $\theta_{\min} > 1.9\ ^oC$. The mesoscale parameter q (Fig. 15b) shows a similar structure. The ridge shown by warmer temperatures has less negative potential vorticity, while the trough shown by cooler temperatures has more negative potential vorticity with a minimum indicating a cyclonic centre. The mean density, $\overline{\sigma_\theta}$ shows very weak contrast with high density in the SE and low values to the NW with the hint of a closed feature near the $\theta_{\min}$ and q

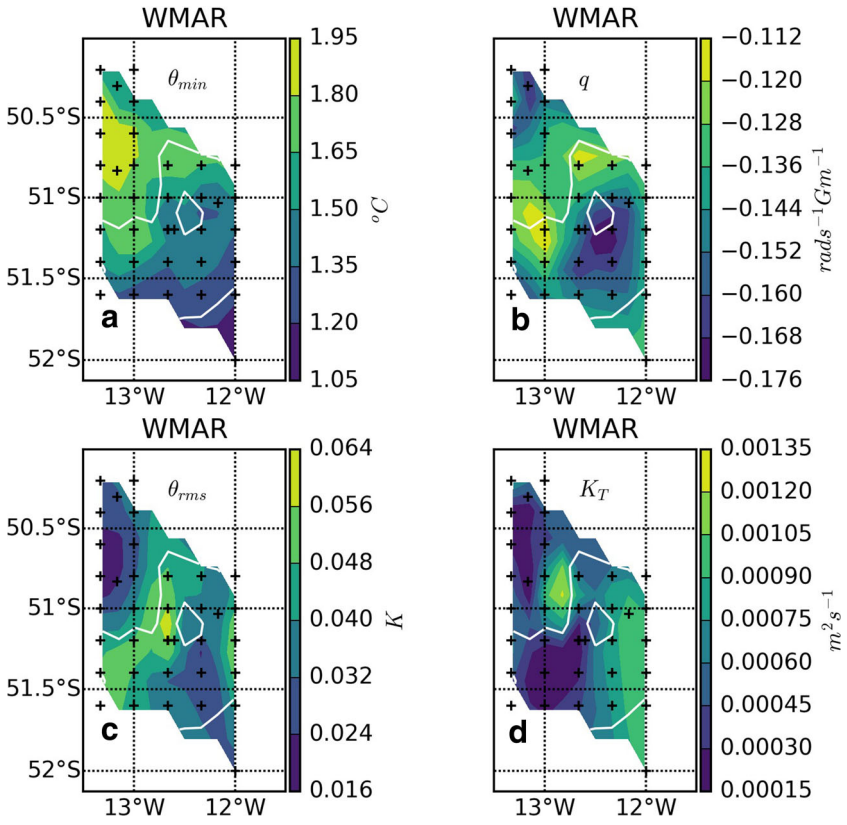

Fig. 15 Maps of parameters for the ANTXXVIII/3 Eddy-Pump West Mid-Atlantic Ridge Survey overlain with the mean potential density $\overline{\sigma_\theta}$ for the upper thermocline depth range 100–480 m with a contour interval of 0.05 kg m^{-3}; the closed contour is a density minimum: **a** potential temperature at the Winter Water potential temperature minimum, $\theta_{\min}$ in ^{o}C, **b** potential vorticity q calculated for the depth range 100–480 m in rad s^{-1} Gm^{-1}, **c** the root mean square variability of potential temperature in pressure coordinates $\theta_{\rm rms}$ in K, **d** the vertical diffusivity based on the Thorpe-scale K_T in $m^2\ s^{-1}$

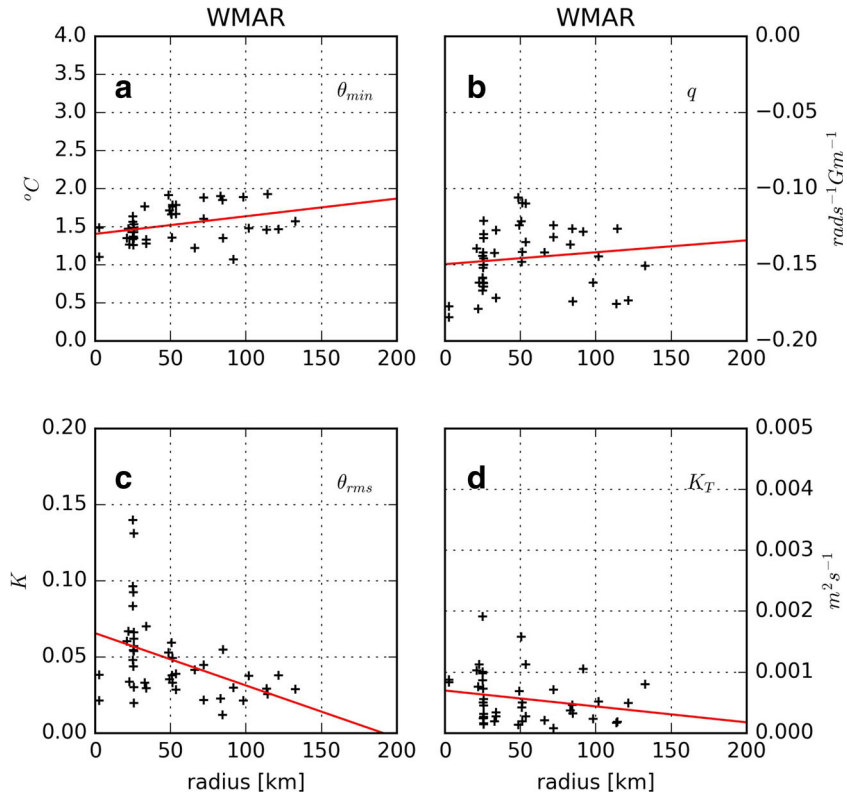

Fig. 16 Plots of parameters for the ANTXXVIII/3 Eddy-Pump West Mid-Atlantic Ridge Survey as a function of the distance from the eddy centre at 51.20^o S, 12.30^o W including the regression line: **a** potential temperature at the Winter Water potential temperature minimum, $\theta_{\min}$ in ^{o}C ($R = 0.346$, $p = 0.023$), **b** potential vorticity calculated for the depth range 100–480 m in rad s^{-1} Gm^{-1} ($R = 0.129$, $p = 0.410$), **c** the root mean square variability of potential temperature in pressure coordinates $\theta_{\rm rms}$ in K ($R = -0.422$, $p = 0.005$), **d** the vertical diffusivity based on the Thorpe-scale K_T in $m^2\ s^{-1}$ ($R = -0.215$, $p = 0.166$)

minima; this feature is a density minumum, as can be seen in the section, Fig. 17, discussed below.

The measures of fine-scale temperature variability, θ_{rms}, (Fig. 15c) shows greater variability on the boundary between the warmer and colder water. The vertical diffusivity based on the Thorpe-scale K_T (Fig. 15h) shows values in the range 2×10^{-4} to 1×10^{-3} m^2 s^{-1}, and its spatial structure shows one high value on the boundary between the warmer and cooler water, though not at the same position as θ_{rms}, and higher values in the east, of which there is only a hint in the other parameters.

Figure 16 shows parameters for the ANTXXVIII/3 Eddy-Pump West Mid-Atlantic Ridge Survey as a function of the distance from the eddy centre at 51.20^o S, 12.30^o W including the regression line. Potential temperature at the WW potential temperature minimum, θ_{min} in ^{o}C (a) (R = 0.346, p = 0.023) shows a significant positive correlation with distance from the eddy centre while potential vorticity calculated for the depth range 100–480 m in rad s^{-1} Gm^{-1} (b) (R = 0.129, p = 0.410) shows a weak positive correlation with distance. The root mean square variability of potential temperature in pressure coordinates θ_{rms} in K (c) (R = − 0.422, p = 0.005) shows a significant negative correlation with distance, but with highest values at a range of 25 km, while the vertical diffusivity based on the Thorpe-scale K_T in $m^2\ s^{-1}$ (d) (R = − 0.215, p = 0.166) shows only a weak negative correlation.

The section along 12^o 20' W, Fig. 17, through the centre of the q minumum east of the centre of the survey area (Fig. 15), is unfortunately shorter than would have been ideal, but does show a rather flattened lens of the WW θ_{min}. The isopycnals below this temperature minimum are bowed downwards, rather than upwards, in this case.

The θS diagram for this survey, Fig. 18, shows a tighter relationship than in all the other cases with the WW θ_{min} in the range 1.1–1.9 ^{o}C. Profiles from close to the centre in darker colours and those further away in paler colours are bundled together.

5 Discussion

During the Eddy-Pump (ANTXXVIII/3) Cruise, we observed that the interleavings were different in magnitude from place to place and wondered whether they were particularly strong in any part of the eddies. However, we found that they were different from eddy to eddy. By looking back at the earlier EIFEX (ANTXXI/3) dataset, in which we had already considered the evolution of some eddy characteristics, and estimating the ages using altimeter data, we gained the impression that the age of the eddy could be used to

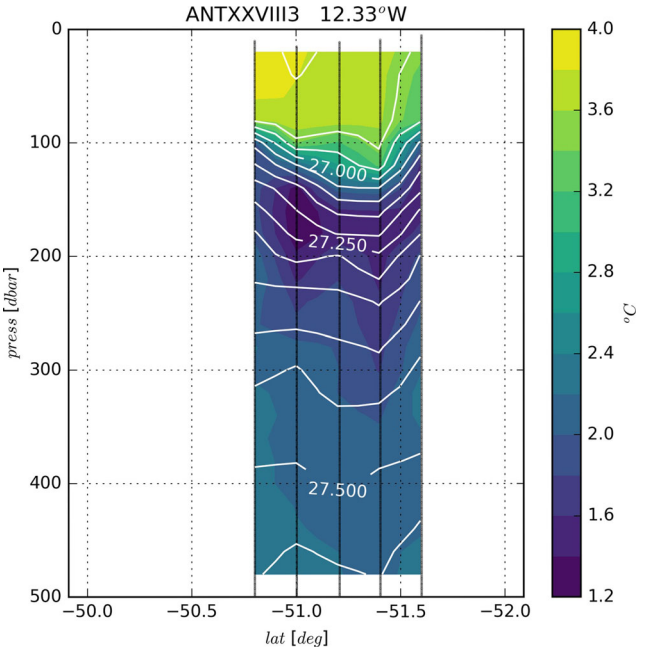

Fig. 17 Meridional section through the ANTXXVIII/3 Eddy-Pump West Mid-Atlantic Ridge Eddy along 12^o 20' W showing potential temperature θ overlain with density σ_θ in the top 500 m in white. Note the lens of cold Winter Water thickest at 51.0^o S and how the isopycnals in this case are actually depressed. For scale 1^o of latitude corresponds to 111 km. The station positions are marked by thin black lines

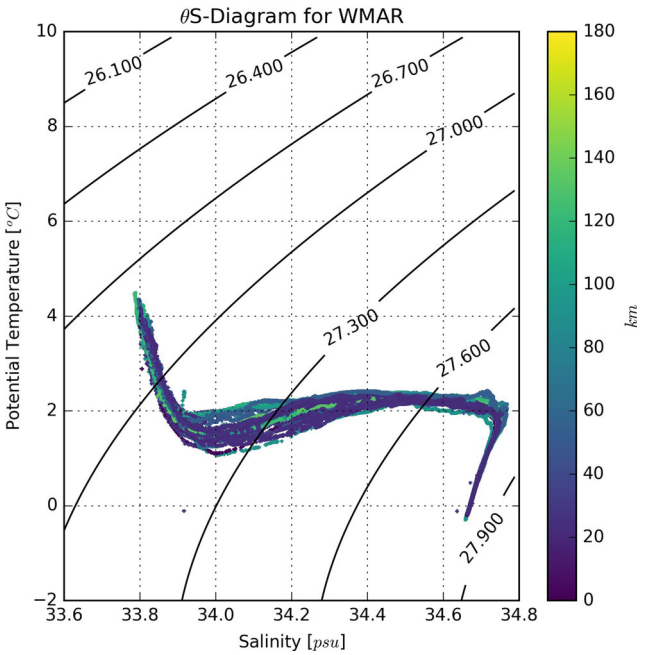

Fig. 18 Potential temperature-salinity, θS, diagram for the ANTXXVIII/3 Eddy-Pump West Mid-Atlantic Ridge Eddy Survey. Contours of potential density, σ_θ, are shown in black. Notice the bundling of local water masses, in particular the Winter Water θ minima in the range 1.0 to 2.0 ^{o}C. The profiles are coloured by the distance from the eddy centre at 51.20^o S, 12.30^o W

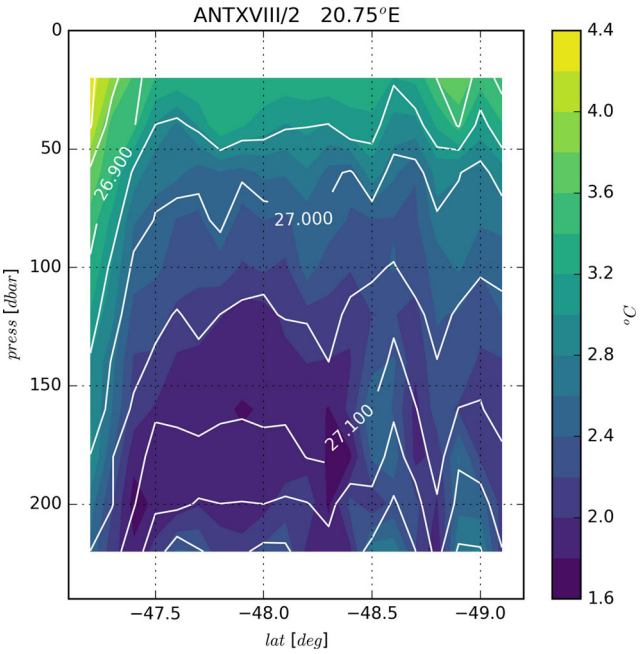

Fig. 19 Meridional sections through the ANTXVIII/2 "EisenEx" cold core eddy along 20^o 45' E showing potential temperature θ overlain with density σ_θ in the top 220 m in white. Note the flattened lens of cold Winter Water centred at about 48.0^o S and how the isopycnals in this case slope steeply down in the north and south; to the south they slope up again where the eddy is detaching from its parental front

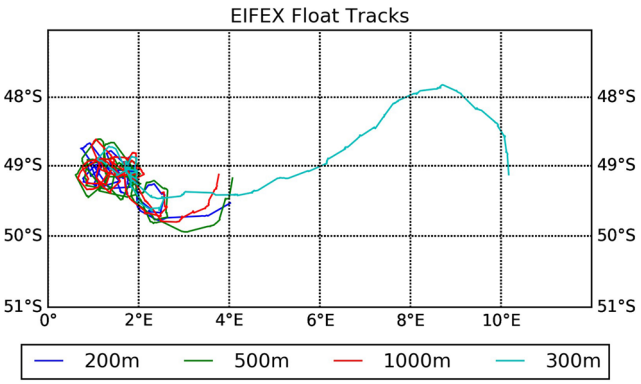

Fig. 20 Tracks of four APEX floats on 31st May 2004 originally released in EIFEX Eddy 2 on 14th and 17th March 2004. The float at 300 m depth crossed the 3^o E meridian on 24th April, while the floats at 200, 500 and 1000 m crossed it on 27th, 25th and 24th May respectively

explain the differences observed. This has allowed us to develop a hypothesis about how eddies evolve.

The mesoscale parameters, $\theta_{\min}$ and q, for all four eddy features (Fig. 3a, b, Fig. 7a, b, Fig. 11a, b, Fig. 15a, b) show a cyclonic cold WW core $\theta_{\min}$ and more negative potential vorticity q. The first three (EIFEX Eddy 1, EP GeoB and EIFEX Eddy 2) also show a denser core, $\overline{\sigma_\theta}$, indicating an upward doming of the isopycnals, as can be seen in the cross-sections through the eddies (Fig. 5, Figs. 9 and 13). However, the last example (EP WMAR) does not share this because, within the depth range observed, the isopycnals are bowed slightly downwards in the centre of the eddy beneath the WW $\theta_{\min}$ (Fig. 17), though the WW $\theta_{\min}$ and more negative potential vorticity q indicate this is, or was, a cyclonic feature. These all show the cold WW $\theta_{\min}$ but with core temperatures of about 0.4 ^{o}C (EIFEX Eddy 1), 0.4 ^{o}C (EP GeoB), 1.0 ^{o}C (EIFEX Eddy 2) and 1.3 ^{o}C (EP WMAR). These eddies all formed between the Antarctic Polar Front and the Southern Polar Front, so that their initial temperatures might be expected to be similar and the increasing temperature a sign of increasing age as reported by Hibbert et al. (2009), with a warming rate of about 0.1 K per month.

Another dataset of interest to the analysis presented here is the survey of the cold core eddy used in the "EisenEx" iron fertilisation experiment, *Polarstern* Cruise ANTXVIII/2 from 25th October to 3rd December 2000 (Strass et al. 2001), where CTD data were collected along five meridional sections across the eddy using a towed Scanfish. The depth range was limited to about 220 m, only just capturing the WW $\theta_{\min}$, so that the analyses of the lowered CTD data presented for the other eddies could not be carried out. However, the section through the middle of the eddy at 20^o 45' E (Fig. 19) shows steep isopycnal slopes at the edge and flattened isopycnals in the centre, more consistent with that of the older eddies. The core temperature is about 1.2 ^{o}C, likewise indicating a more mature structure. The altimeter data show a rather complicated history. A cyclonic feature becomes established here in June 2000. During July, it wanders to the southern boundary of this area, but returns. At the beginning of October, it joins another cyclonic feature approaching from the west, which eventually replaces it (see, Supplementary Material 5_EisenEx_Eddy.mov).

The fine-scale potential temperature parameter θ_{rms} (Fig. 3c, Fig. 7c, Fig. 11c and Fig. 15c) shows a variety of different distributions. The first survey (EIFEX Eddy 1) show greater rms variability of potential temperature θ_{rms} in the core of the eddy. The next survey (EP GeoB) shows a maximum off centre and the last two, (EIFEX Eddy 2 and EP WMAR) show greater variability around the edge of the cold core.

In the recently formed cyclonic eddy with a cold WW core observed by Joyce et al. (1981) in Drake Passage, they report enhanced interleaving around the edge of the eddy, as do Adams et al. (2017) from a new eddy in the Scotia Sea, though their data does not include the eddy centre; our younger eddies show more variability in the centre. In their study of anticyclonic lenses of Mediterranean Outflow Water ("Meddies") in the North Atlantic, Armi and Zenk (1984) also comment on the enhanced fine-scale variability

round the edge of the eddy and reduced variability in the centre, as do Pietri and Karstensen (2018) for an SCV in the eastern tropical North Atlantic; by comparison, these features are very old, maybe even years; this result agrees better with our observations.

The vertical eddy diffusivity based on the Thorpe-scale method, K_T, (Fig. 3d, Fig. 7d, Fig. 11d and Fig. 15d) shows largest values within the eddy core in the first case (EIFEX Eddy 1). In the second case (EP GeoB), the largest value is in the core, though there are local maxima around the edge. In the third case (EIFEX Eddy 2), there are local maxima around the edge of the eddy, while in the fourth case (EP WMAR), the largest values are away from the core of the small weak eddy feature. In all four surveys, the values of K_T in the upper thermocline are roughly in the range 10^{-4} to 10^{-3} m^2 s^{-1}. This is in reasonable agreement with measurements made using the MSS free-falling turbulence sonde during the EIFEX and Eddy-Pump cruises as well as the earlier EisenEx cruise (Cisewski et al. 2005, 2008; Strass et al. 2017a, b). The values presented here were simply obtained using the processed CTD data, rather than using the more detailed analysis techniques based on raw data as advocated by Gargett and Garner (2008), so they may not be such a good estimate of K_T. However, in this study, we are more concerned with the spatial distribution of the fine-scale variability, and it is interesting to see that they do agree with the θ_{rms} distributions in both the younger and older eddies. The shift of the K_T maximum to the rim of the eddies as they age supports the idea that this is where the stronger shears are concentrated in the older eddies. Because of the enhanced horizontal density gradient there will be, due to the geostrophic relationship, enhanced vertical shear, which in its turn provides greater opportunity for overturnings.

The diagrams showing the values of parameters as a function of distance from the eddy centre (Figs. 4, 8, 12 and 16) all show θ_{min} increasing and q becoming less negative away from the centre (a, b). The first two cases (EIFEX Eddy 1 and EP GeoB) show both θ_{rms} and K_T decreasing away from the eddy centre, while the third case (EIFEX Eddy 2) shows both of these measures increasing away from the eddy centre. The fourth case (EP WMAR) shows the largest values of θ_{rms} and K_T in the distance range 25–50 km which corresponds to the distance to the eddy centre of the weak frontal feature which runs across the area. The large number of data points there are due to the repeated measurements made at the "central station" of this survey area at 51^o 12' S, 12^o 40' W, the temporal development at which is documented in Strass et al. (2017a, b).

The θS diagrams (Figs. 6, 10, 14 and 18) show a general trend from case to case, EIFEX Eddy 1 → EP GeoB → EIFEX Eddy 2 → EP WMAR, of reduced variability and greater organisation, which would be consistent with a general homogenisation of water mass properties within the core of the eddy as time passes, though it should be noted that while the first three surveys extended to about 160 km from their notional centre, the last one only extended to about 120 km. Also, the profiles from the centres of the eddies, as depicted by the dark blue curves, show the "knee" of the WW becoming less pronounced. As explained by Hibbert et al. (2009), homogenisation is effected principally by lateral or isopycnic stirring and mixing processes; diapycnic mixing alone would only warm the local θ_{min} values without homogenising them.

As witnessed by those eddies discussed here, and seen more generally in Chelton et al. (2011) statistics, eddies have a lifetime of weeks to months. Figure 20 shows the tracks of four APEX floats on 31st May 2004 originally released in EIFEX Eddy 2 on 14th and 17th March 2004. The float at a 300-m depth crossed the 3^o E meridian on 24th April, while the floats at 200, 500 and 1000 m crossed it on 27th, 25th and 24th May respectively indicating a collapse of the eddy just over 2 months following the end of the experiment. This eddy lifetime is comparable to the natural time-scale of plankton blooms in the ACC, which is weeks (Smetacek et al. 2012; Soppa et al. 2016; Hoppe et al. 2017). Thus, the homogenisation of physical properties within the eddy described here will be important for biogeochemical properties and distributions too. Nutrients may become depleted, so that during the relatively long lifetime of the eddies the rate at which productivity can proceed will be constrained by vertical diffusive fluxes.

6 Conclusions

Our youngest eddy shows isopycnals which are domed upwards and a variety of waters with differing temperature-salinity characteristics in its core. The older eddies show cores which are increasingly homogeneous with age. The isopycnals in the older eddies are more flattened in the centre of the eddy and in cross-section they can be M-shaped, so that the steepest gradients are concentrated around the rim of the eddy. We hypothesise that stirring and mixing processes within the eddy are likely to homogenise the water so that the temperature-salinity relationship becomes tighter. Fine-scale variability, characterised by θ_{rms} and K_T, which is spread throughout the youngest eddy, becomes concentrated around the edges of the older eddies, so that younger eddies have more variability in the centre and older eddies more round the edge.

To test our hypothesis about how eddies evolve properly would require detailed study of a series of similar eddies with different ages. As is so often in ocean science, the

dataset available to us was not ideal and new experiments collecting more systematic datasets would probably be needed. This might not be so simple. Argo floats are probably too sparse, but have essentially vertical profiles. Gliders and towed systems would be inclined to muddle horizontal and vertical variability, so that a number of time-consuming high-resolution CTD surveys might be required. Alternatively, by combining Argo float data with altimeter data, it might be possible to test our hypothesis, if sufficient profiles could be found and their positions relative to the centre of eddies of known age determined.

The sharpened front-like gradients around the edge offer the opportunity for baroclinic and barotropic instability to cause the eddy to collapse and release the water it has homogenised back into the general flow, as illustrated by the release of the floats from EIFEX Eddy 2 (Fig. 20). We can see from this how the formation of eddies, homogenisation of properties within them and the release of this modified water could contribute to the way in which ocean processes are changing water mass characteristics.

The correct representation of the processes described in this paper is going to be important for modelling not only of the bulk rate at which the ocean is converting and exchanging water mass properties such as heat and fresh water but also of biogeochemical processes which depend on this physical context.

Acknowledgements Our thanks are due to Chris Hughes and Angela Hibbert at the National Oceanography Centre in Liverpool for extracts of the Aviso merged altimetric data set and to Santiago Gonzalez at NIOZ for the data from the Scanfish towed system (ANTXVIII/2).

Funding information This study is supported by the German Federal Ministry for Education and Research (Bundesministerium für Bildung und Forschung, BMBF) for funding *Polarstern* and this ship's captains and crews. HL's travel costs were born by the Royal Society (ANTXVIII/2, ANTXXI/3) and the School of Environmental Sciences (ANTXXVIII/3).

References

Adams KA, Hosegood P, Taylor JR, Sallée J-B, Bachman S, Torres R, Stamper M (2017) Frontal circulation and submesoscale variability during the formation of a Southern Ocean mesoscale eddy. J Phys Oceanogr 47:1737–1753. https://doi.org/10.1175/JPO-D-16-0266.1

Armi L, Zenk W (1984) Large lenses of highly saline mediterranean water. J Phys Oceanogr 14:1560–1576

Behrenfeld MJ (2010) Abandoning Sverdrup's critical depth hypothesis on phytoplankton blooms. Ecol 91:977–989

Bopp L, Lévy M, Resplandy L, Sallée JB (2015) Pathways of anthropogenic carbon subduction in the global ocean. Geophys Res Lett 42:6416–6423. https://doi.org/10.1002/2015GL065073

Charney JG (1947) The dynamics of long waves in a baroclinic westerly current. J Meteor 4:135–162

Chelton DB, Schlax MG, Samelson RM (2011) Global observations of nonlinear mesoscale eddies. Prog Oceanogr 91(2):167–216. https://doi.org/https://doi.org/10.1016/j.pocean.2011.01.002

Cisewski B, Strass VH, Prandke H (2005) Upper-ocean vertical mixing in the Antarctic Polar Front Zone. Deep-Sea Res II 52:1087–1108. https://doi.org/10.1016/j.dsr2.2005.01.010

Cisewski B, Strass VH, Losch M, Prandke H (2008) Mixed layer analysis of a mesoscale eddy in the Antarctic Polar Front Zone. J Geophys Res 113:C05017. https://doi.org/10.1029/2007JC004372

D'Asaro EA (1988) Generation of submesoscale vortices: a new mechanism. J Geophys Res 93:6685–6693

Eady ET (1949) Long waves and cyclone waves. Tellus 1:258–277

Edmon HJ, Hoskins BJ, McIntyre ME (1980) Eliassen-Palm cross-sections for the troposphere. J Atmos Sci 2600-2616:37. (see also Corrigendum, J. Atmos. Sci., 38, 1115, 1980)

Fischer J, Leach H, Woods JD (1989) A synoptic map of isopycnic potential vorticity in the seasonal thermocline. J Phys Oceanogr 19:519–531

Gargett A, Garner T (2008) Determining Thorpe scales from ship-lowered CTD density profiles. J Atmos and Ocean Tech 25:1657–1670. https://doi.org/10.1175/2008JTECHO541.1

Gill AE, Green JSA, Simmons AJ (1974) Energy partition in the large-scale ocean circulation and the production of mid-ocean eddies. Deep-Sea Res 21:499–528

Gordon AL (1971) Antarctic Polar Front Zone. Antarctic Oceanology, Vol. 1, Antarctic Research Series, J. L. Reid, Ed., Amer. Geophys. Union, 205–221

Gordon AL, Georgi DT, Taylor HW (1977) Antarctic polar frontal zone in the western Scotia Sea - summer 1975. J Phys Oceanogr 7:309–328

Hibbert A, Leach H, Strass V, Cisewski B (2009) Mixing in cyclonic eddies in the Antarctic Circumpolar Current. J Mar Res 67:1–23. https://doi.org/10.1357/002224009788597935

Hoppe C, Klaas C, Ossebaar S, Soppa MA, Cheah W, Laglera L, Santos-Echeandia J, Rost B, Wolf-Gladrow D, Bracher A, Hoppema M, Strass V, Trimborn S (2017) Controls of primary production in two phytoplankton blooms in the Antarctic Circumpolar Current. Deep Sea Res Part II: Top Stud Oceanogr 138:63–73. https://doi.org/10.1016/j.dsr2.2015.10.005

Ito T, Parekh P, Dutkiewicz S, Follows MJ (2005) The Antarctic circumpolar productivity belt. Geophys Res Lett 32:L13604. https://doi.org/10.1029/2005GL023021

Jones EM, Hoppema M, Strass V, Hauck J, Salt L, Klaas C, van Heuven SMAC, Wolf-Gladrow D, de Baar HJW (2017) Mesoscale features create hotspots of carbon uptake in the antarctic circumpolar current. Deep Sea Res Part II: Top Stud Oceanogr 138:39–51

Joyce T (1977) A note on the lateral mixing of water masses. J Phys Oceanogr 7:626–629

Joyce T, Zenk W, Toole JM (1978) The anatomy of the Antarctic polar front in the Drake Passage. J Geophys Res 83:6093–6113

Joyce TM, Patterson SL, Millard RC (1981) Anatomy of a cyclonic ring in the Drake Passage. Deep Sea Res 28:1265–1287

Kurczyn JA, Beier E, Lavín MF, Chaigneau A, Godínez VM (2013) Anatomy and evolution of a cyclonic mesoscale eddy observed in the northeastern Pacific tropical-subtropical transition zone. J Geophys Res Oceans 118:5931–5950. https://doi.org/10.1002/2013JC009339

Leach H, Strass VH, Cisewski B (2011) Modification by lateral mixing of the Warm Deep Water entering the Weddell Sea in the Maud Rise region. Ocean Dyn 61(1):51–68. https://doi.org/10.1007/s10236-010-0342-y

MacVean MK, Woods JD (1980) Redistribution of scalars during upper ocean frontogenesis. a numerical model. Quart J Roy Met Soc 106:293–311

Marshall J, Speer K (2012) Closure of the meridional overturning circulation through Southern Ocean upwelling. Nat Geosci 5:171–180. https://doi.org/10.1038/NGEO1391

Martin JH (1990) Glacial-interglacial CO_2 change: the iron hypothesis. Paleoceanography 5:1–13

McWilliams JC (1985) Submesoscale, coherent vortices in the ocean. Rev Geophys 23:165–182

Methven J (1998) Spirals in potential vorticity. Part II: Stability J Atmos Sci 55:2067–2079

Methven J, Hoskins BJ (1998) Spirals in potential vorticity. Part 1: Measures of Structures J Atmos Sci 55:2053–2066

Methven J, Hoskins BJ (1999) The advection of high-resolution tracers by low-resolution winds. J Atmos Sci 56:3262–3285

Meunier T, Ménesguen C., Schopp R, le Gentil S (2015) Tracer stirring around a meddy: the formation of layering. J Phys Oceanogr 45:407–423. https://doi.org/10.1175/JPO-D-14-0061.1

MODE-Group (1978) The mid-ocean dynamics experiment. Deep-Sea Res 25:859–910

Molemaker MJ, McWilliams JC, Dewar WK (2015) Submesoscale instability and generation of mesoscale anticyclones near a separation of the California undercurrent. J Phys Oceanogr 45:613–629. https://doi.org/10.1175/JPO-D-13-0225.1

Moore JK, Abbott MR (2000) Phytoplankton chlorophyll distributions and primary production in the Southern Ocean. J Geophys Res 105, 28:709–28, 722

Moore JK, Abbott MR (2002) Surface chlorophyll concentrations in relation to the antarctic polar front: seasonal and spatial patterns from satellite observations. J Mar Systems 37:69–86

Munk WH (1950) On the wind-driven circulation. J Meteorol 7:79–93

Orsi AH, Whitworth T III, Nowlin WD Jr (1995) On the meridional extent and fronts of the Antarctic Circumpolar Current. Deep-Sea Res I 42:641–673

Peterson RG, Nowlin WD, Whitworth T (1982) Generation and evolution of a cyclonic ring at Drake Passage in early 1979. J Phys Ocean 12:712–719

Peterson RG, Whitworth T (1989) The Subantarctic and Polar Fronts in relation to deep water masses through the southwestern Atlantic. J Geophys Res 94:10817–10838

Pietri A, Karstensen J (2018) Dynamical characterisation of a low oxygen submesoscale coherent vortex in the Eastern North Atlantic Ocean. J Geophys Res.: Oceans 123:2049–2065. https://doi.org/10.1002/2017JC013177

Sallée JB, Matear RJ, Rintoul SR, Lenton A (2012) Localized subduction of anthropogenic carbon dioxide in the Southern Hemisphere oceans. Nat Geosci 5(8):579–584. https://doi.org/10.1038/ngeo1523

Smetacek V (2005) Fahrtabschnitt ANT XXI/3 Kapstadt-Kapstadt. Ber Polarforsch Meeresforsch 500:1–134

Smetacek V, Klaas C, Strass VH, Assmy P, Montresor M, Cisewski B, Savoye N, Webb A, d'Ovidio F, Arrieta JM, Bathmann U, Bellerby R, Berg GM, Croot P, Gonzalez S, Henjes J, Herndl GJ, Hoffmann LJ, Leach H, Losch M, Mills MM, Neill C, Peeken I, Röttgers R, Sachs O, Sauter E, Schmidt MM, Schwarz J, Terbrüggen A, Wolf-Gladrow D (2012) Deep carbon export from a Southern Ocean iron-fertilized diatom bloom. Nature 487:313–319. https://doi.org/10.1038/nature11229

Smith KS, Ferrari R (2009) The production and dissipation of compensated thermohaline variance by mesoscale stirring. J Phys Oceanogr 39:2477–2501. https://doi.org/10.1175/2009JPO4103.1

Sokolov S, Rintoul SR (2009) Circumpolar structure and distribution of the Antarctic Circumpolar Current fronts: 1. Mean circumpolar paths. J Geophys Res 114:C11018. https://doi.org/10.1029/2008JC005108

Soppa M, Völker C, Bracher A (2016) Diatom phenology in the southern ocean: mean patterns, trends and the role of climate oscillations. Remote Sensing 8(420):1–17. https://doi.org/10.3390/rs8050420 , hdl:10013/epic.47911

Stommel H (1948) The westward intensification of wind-driven ocean currents. Eos Trans AGU 29:2002–206. https://doi.org/10.1029/TR029i002p00202

Strass VH, Leach H, Cisewski B, Gonzalez S, Post J, da Silva Duarte V, Trumm F (2001) The physical setting of the Southern Ocean Iron Fertilisation Experiment. Chapter 10. In: Smetacek V, Bathmann U, El Naggar S (eds) 2001, The Expeditions ANTARKTIS XVIII/1-2 of the Research Vessel "Polarstern" in 2000. Berichte zur Polar- und Meeresforschung, Nr 400. 232pp

Strass VH, Naveira Garabato AC, Pollard RT, Fischer HI, Hense I, Allen JT, Read JF, Leach H, Smetacek V (2002) Mesoscale frontal dynamics: shaping the environment of primary production in the Antarctic Circumpolar Current. Deep-Sea Res II 49(18):3735–3770. https://doi.org/10.1016/S0967-0645(02)00109-1

Strass V, Cisewski B, Gonzales S, Leach H, Loquay K-D, Prandke H, Rohr H, Thomas M (2005) The physical setting of the European iron fertilization experiment 'EIFEX' in the Southern Ocean. Rep Polar Mar Res 500:15–49

Strass VH, Leach H, Prandke H, Donnelly M, Bracher AU, Wolf-Gladrow DA (2017a) The physical environmental conditions for biogeochemical differences along the Antarctic Circumpolar Current in the Atlantic Sector during late austral summer 2012. Deep-Sea Res II(138):6–25. https://doi.org/10.1016/j.dsr2.2016.05.018

Strass V, Pakhomov E, Wolf-Gladrow D (2017b) Eddy-Pump: pelagic processes along the eddying Antarctic Polar Front with influence on the carbon pump in the Atlantic Sector of the Southern Ocean. Deep-Sea Res II 138:1–140

Sverdrup HU (1947) Wind-driven currents in a baroclinic ocean; with application to the equatorial currents of the eastern Pacific. Proc Natl Acad Sci USA 33(11):318–26. https://doi.org/10.1073/pnas.33.11.318

Swart NC, Ansorge IJ, Lutjeharms JRE (2008) Detailed characterization of a cold Antarctic eddy. J Geophys Res 113:C01009. https://doi.org/10.1029/2007JC004190

Thompson AF, Gille ST, MacKinnon JA, Sprintall J (2007) Spatial and temporal patterns of small-scale mixing in Drake Passage. J Phys Oceanogr 37:572–592. https://doi.org/10.1175/JPO3021.1

Thomsen S, Kanzow T, Krahmann G, Greatbatch RJ, Dengler M, Lavik G (2016) The formation of a subsurface anticyclonic eddy in the Peru-Chile undercurrent and its impact on the near-coastal salinity, oxygen and nutrient distributions. J Geophys Res: Oceans 121:476–501. https://doi.org/10.1002/2015JC010878

Thorpe SA (1977) Turbulence and mixing in a Scottish Loch. Phil Trans Roy Soc London 286A:125–181

Wolf-Gladrow D (2013) The expedition of the research vessel "Polarstern" to the Antarctic. In: 2012 (ANT-XXVIII/3). Ber. Pol. u. Meeresf., 661, 195 pp. http://hdl.handle.net/10013/epic.41332

Woods JD, Onken R, Fischer J (1986) Thermohaline intrusions created isopycnally at oceanic fronts are inclined to isopycnals. Nature 322:446–449

Zhang Z, Tian J, Qiu J, Zhao W, Chang P, Wu D, Wan X (2016) Observed 3D structure, generation, and dissipation of oceanic mesoscale eddies in the South China Sea. Sci Rep 6:24349. https://doi.org/10.1038/srep24349